expression of nuclear and mitochondrial genes encoding mitochondrial proteins, respectively. *PGC-1* mRNA is induced in both BAT and skeletal muscles upon exposure of the animals to low temperature (*16*). The induction of *PGC-1* by cold exposure is mediated through β adrenergic receptors in BAT, but the mechanisms controlling *PGC-1* expression in skeletal muscles are not known.

We observed an increase of *PGC-1* expression in skeletal muscles of CaMKIV* transgenic mice (Fig. 1C). A 3-kb proximal promoter region from the human *PGC-1* gene was activated by a factor of 4 by CaMKIV* in C2C12 myocytes; this result suggests that CaMK signaling can induce PGC-1 gene expression at a transcriptional level (Fig. 1E). CaMKIV activates several transcription factors, such as CREB (cyclic adenosine monophosphate responsive element-binding protein) and MEF2 (myocyte-specific enhancer factor 2) (*13, 19, 20*); identification of the specific transcription factors responsible for the effect of CaMK on transcription of the *PGC-1* gene will require further investigation.

The expression of mitochondrial genes among specialized myofiber subtypes is proportionate to mitochondrial DNA copy number (*1*). Mitochondrial DNA copy number per nuclear genome was increased in skeletal muscles of MCK-CaMKIV* transgenic mice (Fig. 2A). Transmission electron microscopy performed on sections prepared from plantaris muscles of wild-type and MCK-CaMKIV* transgenic mice revealed that the mitochondria of oxidative myocytes of control plantaris occupied 24 ± 4% of the total cross-sectional area of the myocyte, whereas in MCK-CaMKIV* plantaris this value was 38 ± 6% ($P < 0.05$). The average thickness of subsarcolemmal mitochondrial collections was significantly higher in the MCK-CaMKIV* plantaris than in control plantaris (1.5 ± 0.4 μm versus 1.0 ± 0.1 μm; $P < 0.05$), as assessed from analysis of at least 200 separate muscle fibers from each group (Fig. 2B).

In wild-type mice (F3 hybrid C57BL/6 × SJL), the average percentage of type I fibers in plantaris muscle was about 2%, whereas in MCK-CaMKIV* transgenic mice, type I fibers accounted for about 10% of the total fibers (Fig. 3, A and B). The changes in gene expression and muscle ultrastructure that occurred as consequence of CaMK activity were accompanied by improved contractile performance (fatigue resistance) during repetitive contractions of isolated muscle (EDL) preparations (*21*) (Fig. 3C).

The ability of the CaMKIV* transgene to increase the abundance of type I fibers resembles the response to activated calcineurin (*10*). However, the induction of *PGC-1*, increased expression of mitochondrial genes, and increased expression of nuclear genes encoding mitochondrial proteins was much greater in CaMKIV*-transgenic mice than in calcineurin-transgenic animals (Fig. 3, D and E). Endogenous CaMKIV is not highly expressed in skeletal muscles (*12*), but CaMKI is abundant in this tissue (*22, 23*), and constitutively active forms of CaMKI and CaMKIV are equally potent in activating target genes in a skeletal myocyte background (Fig. 3F).

Overall, our data suggest that CaMK mediates contractile activity-dependent gene regulation in muscle tissues and promotes mitochondrial biogenesis. Further studies will be required to identify the specific CaMK isoform and the specific substrates of CaMK responsible for these effects. Habitual patterns of physical activity have profound effects on human performance in athletes, in healthy individuals during normal aging, and in patients with chronic diseases such as congestive heart failure or respiratory insufficiency. Greater understanding of the molecular signaling pathways by which skeletal muscles sense and respond to changing activity patterns by altering programs of gene expression ultimately may promote the development of novel measures to enhance human performance.

References and Notes

1. R. S. Williams, *J. Biol. Chem.* **261**, 12390 (1986).
2. H. Wang, W. R. Hiatt, T. J. Barstow, E. P. Brass, *Eur. J. Appl. Physiol. Occup. Physiol.* **80**, 22 (1999).
3. D. A. Hood, *J. Appl. Physiol.* **90**, 1137 (2001).
4. R. S. Williams, S. Salmons, E. A. Newsholme, R. E. Kaufman, J. Mellor, *J. Biol. Chem.* **261**, 376 (1986).
5. D. Pette, G. Vrbova, *Rev. Physiol. Biochem. Pharmacol.* **120**, 115 (1992).
6. E. R. Chin *et al.*, *Genes Dev.* **12**, 2499 (1998).
7. G. Y. Wu, K. Deisseroth, R. W. Tsien, *Proc. Natl. Acad. Sci. U.S.A.* **98**, 2808 (2001).
8. A. Alevizopoulos, Y. Dusserre, U. Ruegg, N. Mermod, *J. Biol. Chem.* **272**, 23597 (1997).
9. H. Wu *et al.*, *EMBO J.* **19**, 1963 (2000).
10. F. J. Naya *et al.*, *J. Biol. Chem.* **275**, 4545 (2000).
11. S. M. Hughes, M. M. Chi, O. H. Lowry, K. Gundersen, *J. Cell Biol.* **145**, 633 (1999).
12. See supplementary material on *Science* Online at www.sciencemag.org/cgi/content/full/296/5566/349/DC1.
13. R. Passier *et al.*, *J. Clin. Invest.* **105**, 1395 (2000).
14. R. S. Williams, M. Garcia-Moll, J. Mellor, S. Salmons, W. Harlan, *J. Biol. Chem.* **262**, 2764 (1987).
15. P. Puigserver *et al.*, *Cell* **92**, 829 (1998).
16. Z. D. Wu *et al.*, *Cell* **98**, 115 (1999).
17. R. B. Vega, J. M. Huss, D. P. Kelly, *Mol. Cell. Biol.* **20**, 1868 (2000).
18. J. J. Lehman *et al.*, *J. Clin. Invest.* **106**, 847 (2000).
19. H. Bito, K. Deisseroth, R. W. Tsien, *Cell* **87**, 1203 (1996).
20. T. A. McKinsey, C. L. Zhang, J. Lu, E. N. Olson, *Nature* **408**, 106 (2000).
21. R. W. Grange *et al.*, *Am. J. Physiol. Cell. Physiol.* **281**, C1487 (2001).
22. B. Haribabu *et al.*, *EMBO J.* **14**, 3679 (1995).
23. M. R. Picciotto, A. J. Czernik, A. C. Nairn, *J. Biol. Chem.* **268**, 26512 (1993).
24. R. W. Ogilvie, D. L. Feeback, *Stain Technol.* **65**, 231 (1990).

25. We thank D. Kelly and E. N. Olson for critical reading of the manuscript and advice, and J. M. Shelton and C. Humphries for histology and technical assistance. Supported by NIH grants AR40849 and HL06296.

31 October 2001; accepted 11 March 2002

Structure of a Cofactor-Deficient Nitrogenase MoFe Protein

Benedikt Schmid,[1]* Markus W. Ribbe,[4]* Oliver Einsle,[1,3] Mika Yoshida,[1,3] Leonard M. Thomas,[2,3] Dennis R. Dean,[5] Douglas C. Rees,[1,3]† Barbara K. Burgess[4]

One of the most complex biosynthetic processes in metallobiochemistry is the assembly of nitrogenase, the key enzyme in biological nitrogen fixation. We describe here the crystal structure of an iron-molybdenum cofactor–deficient form of the nitrogenase MoFe protein, into which the cofactor is inserted in the final step of MoFe protein assembly. The MoFe protein folds as a heterotetramer containing two copies each of the homologous α and β subunits. In this structure, one of the three α subunit domains exhibits a substantially changed conformation, whereas the rest of the protein remains essentially unchanged. A predominantly positively charged funnel is revealed; this funnel is of sufficient size to accommodate insertion of the negatively charged cofactor.

The two-component enzyme nitrogenase provides the biochemical machinery for the reduction of dinitrogen to ammonia (*1–7*). Biosynthesis of both components, the Fe protein and the MoFe protein, is a complex process, requiring at least 15 different gene products. The MoFe protein (*8*), an $\alpha_2\beta_2$ tetramer, contains in each αβ half two complex metal clusters that are unique in biology and that have yet to be chemically synthesized. One, designated the P cluster, is an [8Fe-7S] cluster that is coordinated by six Cys ligands and bridges the α and β subunits. The other, designated FeMo cofactor (FeMoco), is a [Mo-7Fe-9S] cluster that also contains an endogenous organic component (homocitrate) and is connected to the protein by only two ligands, a Cys and a His, located within the α subunit. The FeMoco represents the site of substrate binding and reduction. In the cell,

the FeMoco is synthesized as a separate, but protein-associated, entity that is subsequently inserted into a P cluster–containing, FeMoco-deficient form of the MoFe protein.

In vitro, it has long been possible to obtain FeMoco by extracting it from the MoFe holoprotein into the organic solvent *N*-methyl formamide (*9*). Recently, it also became possible to purify large quantities of a His-tag version (*10*) of the inactive FeMoco-deficient, but P cluster–containing, MoFe protein from a Δ*nifB* strain (*11*). The *nifB* gene encodes for a protein involved in the biosynthesis of an iron and sulfur–containing precursor of FeMoco (*1*). The in vitro addition of isolated FeMoco to the cofactor-deficient MoFe protein from a Δ*nifB* strain results in an active holoprotein without the requirement of any other factors. Because the FeMoco site is fully buried ~10 Å below the surface of the MoFe protein (*8*), this final cofactor insertion reaction must involve substantial conformational rearrangements in the protein. In this study, the structure of the FeMoco-deficient MoFe protein from an *Azotobacter vinelandii* Δ*nifB* strain (Δ*nifB*-Av1) has been solved to 2.3 Å resolution, revealing the pathway through which the FeMoco is inserted in the final step of MoFe protein assembly.

The determination of the Δ*nifB*-Av1 structure is summarized in Table 1. As is the case for the MoFe holoprotein (Av1), the Δ*nifB*-Av1 $\alpha_2\beta_2$ tetramer consists of a pair of αβ dimers that are related by a molecular twofold rotation axis (Fig. 1A). In contrast to all crystal forms of MoFe proteins observed so far, in the Δ*nifB*-Av1 crystal form, this molecular twofold axis is also crystallographic. The homologous α and β subunits of both Δ*nifB*-Av1 (Fig. 1B) and Av1 (Fig. 1C) consist of three domains each, designated αI, αII, and αIII, and βI, βII, and βIII, respectively. All domains are organized around a common core composed of a four-stranded, parallel β sheet flanked with α helices and additional β strands (*5*). Previous structures have shown that the P cluster, located between domains αI and βI, can exhibit different conformations that likely correspond to different oxidation states (*12, 13*). The conformation of the P cluster observed in the Δ*nifB*-Av1 structure, as isolated and crystallized in the presence of dithionite, is assigned to the P^N state. In Av1 (Fig. 1C), the FeMoco occupies a cavity formed between domains αI, αII, and αIII, which is empty in Δ*nifB*-Av1 (Fig. 1B). A comparison between the structures of Av1 and Δ*nifB*-Av1 shows only minor differences in the β subunit and domains αI and αII, whereas domain αIII undergoes major structural rearrangements (Fig. 2A) (*14*).

The αIII domain in Av1 is organized around a six-stranded β sheet composed of a parallel arrangement of the five β strands shown in Fig. 2, in the order 5, 4, 1, 2, 3, and a sixth antiparallel strand (designated 1′), consisting of residues α31 to α35, which is located adjacent to β strand 3 (*8*). The C_α positions and secondary structure elements of Δ*nifB*-Av1 relative to those of Av1 in the region of the αIII domain that includes α345 to the COOH-terminus are shown in Fig. 2A. A superposition of the polypeptide folds of the two structures in this same region is shown in Fig. 2B. The two β strands 1′ (not shown) and 3, at one end of the six-stranded β sheet in Av1, are disordered in Δ*nifB*-Av1, whereas the remaining β strands are shorter toward their COOH-terminus relative to those in Av1, with the largest positional changes observed for β strands 1 and 2, which are spatially closest to the disordered region. Accompanying these changes, α helices A, C, and D in the αIII domain of Δ*nifB*-Av1 are shorter toward their NH_2-terminus, relative to Av1. The region including the disordered residues α381 to α407 corre-

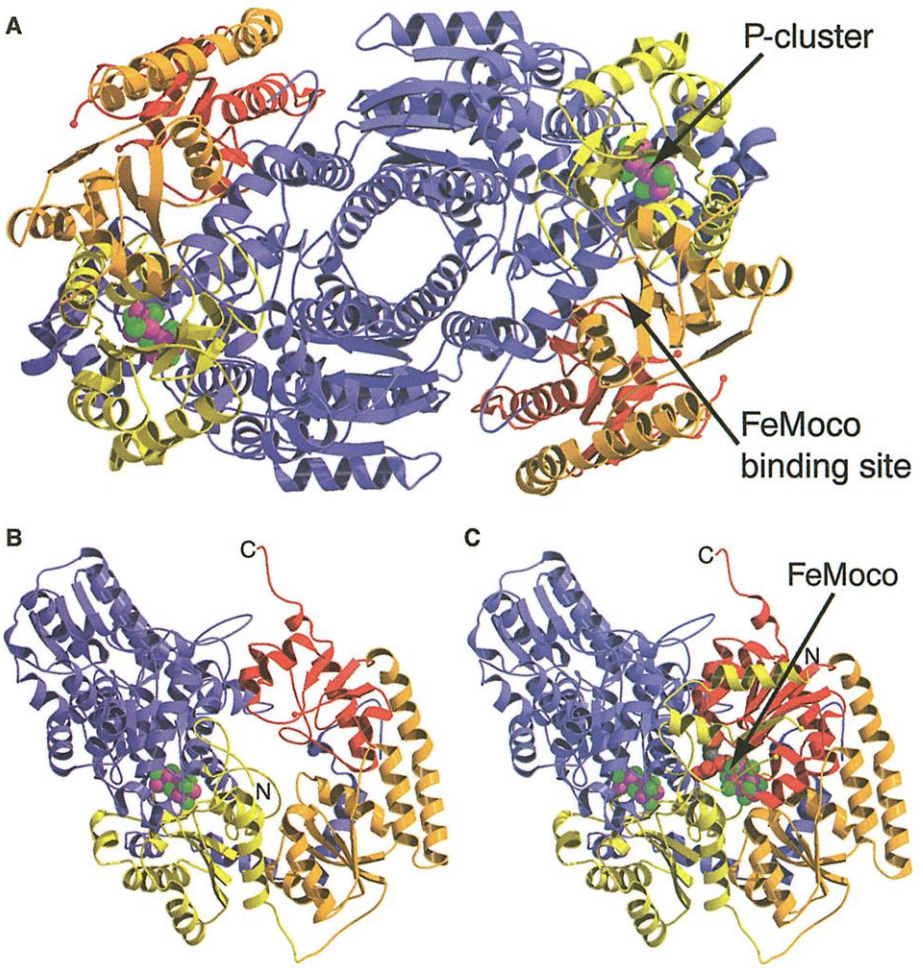

Fig. 1. (**A**) Structure of the Δ*nifB*-Av1 tetramer with the α subunit domains in yellow (αI), orange (αII), and red (αIII) and the β subunits in blue. Residues α380 and α408 are shown as small red spheres, indicating the disordered region in domain αIII (α381 to α407). The P cluster is illustrated as a space-filling model and is color coded by atom, with Fe in purple and S in green. (**B**) Front-side view of one Δ*nifB*-Av1 αβ pair, color coded as in (A). Residues α49 and α480 are labeled N and C, respectively, representing the visible termini of the α subunit in the Δ*nifB*-Av1 structure. (**C**) Front-side view of one Av1 αβ pair (Protein Data Bank entry 3MIN) with the P cluster and the FeMoco illustrated as space-filling models, color coded by atom, with Fe in purple, S in green, O in red, and C in gray (the Mo atom is not visible). The β subunit and the α subunit domains are colored as in (A), with residues α5 to α48 (part of domain αIII) in yellow. Residues α5 and α480 are labeled N and C, respectively, representing the visible termini of the α subunit in the Av1 structure. Residues α35 and α45 are shown as small yellow spheres indicating a disordered region (α36 to α44). The programs MOLSCRIPT (*29*) and RASTER3D (*30*) were used to prepare Figs. 1, 2B, and 3.

[1]Division of Chemistry and Chemical Engineering, Mail Code 147–75CH; [2]Division of Biology, Mail Code 156–29; [3]Howard Hughes Medical Institute, California Institute of Technology, Pasadena, CA 91125, USA. [4]Department of Molecular Biology and Biochemistry, University of California, Irvine, CA 92697–3900, USA. [5]Department of Biochemistry, Virginia Polytechnic Institute and State University, Blacksburg, VA 24061, USA.

*These authors contributed equally to this work.
†To whom correspondence should be addressed. E-mail: dcrees@caltech.edu

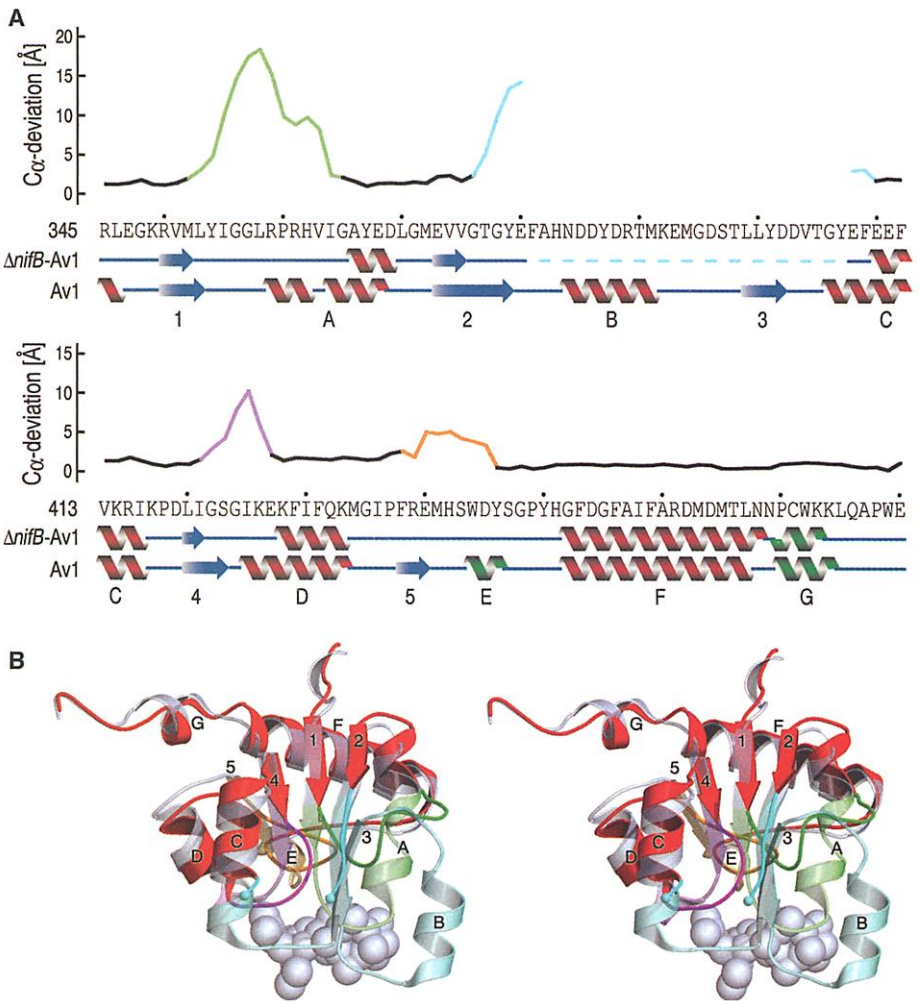

Fig. 2. (**A**) Deviation in C_α positions for residues in domain αIII between Δ*nifB*-Av1 and Av1 after least squares superposition of C_α positions in domains αI and αII with the program LSQMAN (*31*). The amino acid sequence (α345 to α480) is indicated along the abscissa (*32*). The lower rows contain a comparison of the secondary structure elements computed with the program DSSP (*33*), with α helices A, B, C, D, and F shown in red, 3_{10} helices E and G shown in dark green, and β strands 1 to 5 shown in blue. The disordered region (α381 to α407) is represented as a broken line. Four regions with substantial deviations in C_α positions are colored green, blue-green, purple, and orange. (**B**) Stereo drawing of a superposition of the αIII domains in Δ*nifB*-Av1 (red) and Av1 including the FeMoco (light gray). In addition, the four regions with sizable shifts in C_α positions are colored as in (A), with a lighter version in the Av1 structure and a darker version in the Δ*nifB*-Av1 structure. The secondary structure elements are labeled corresponding to (A). Residues α380 and α408 in Δ*nifB*-Av1 are shown as small blue-green spheres, indicating the disordered region between these residues that is not shown.

sponds to the site of an ~50-residue insertion in the MoFe protein from *Clostridium pasteurianum* (*15*), which folds as a large external loop without changing the αIII domain arrangement.

These conformational changes in the αIII domain have important consequences for the region of the MoFe protein involved in FeMoco binding. Selected residues in the FeMoco site are illustrated in Fig. 3 for comparison of the Δ*nifB*-Av1 and Av1 structures. In Av1, the FeMoco is coordinated by only two ligands, His α442 to the Mo atom and Cys α275 to the Fe atom that is located on the opposite side of the cluster from the Mo atom. As Cys α275 is part of domain αII that is unaltered in Δ*nifB*-Av1, it occupies the same position in both structures. In contrast, the C_α of His α442 shifts by ~5 Å during the αIII domain rearrangement. In Δ*nifB*-Av1, it joins two other residues, His α274 and His α451, to form a striking His triad. His α442 is strictly conserved, and histidines are found at positions α274 and α451 in ~80% of known MoFe protein sequences (*16*). Coupled to this rearrangement, residues His α442 and Trp α444 switch their relative positions between Δ*nifB*-Av1 and Av1. Trp α444 is present in ~80% of known sequences (*16*) and is replaced by a Tyr residue in all other sequences. Substantial changes take place in nonliganding residues as well, particularly the stretch from α355 to α359 with Gly α356, Gly α357, and Arg α359 that hydrogen-bond to sulfurs of the cofactor in the holoprotein. At the homocitrate end of the FeMoco, the position of Lys α426 shifts between Av1 and Δ*nifB*-Av1 (Fig. 3).

A comparison of the molecular surfaces of Δ*nifB*-Av1 (Fig. 4A) and Av1 (Fig. 4B) demonstrates that the residue rearrangements occurring in domain αIII create a funnel that allows entry of the FeMoco into the MoFe protein. Despite the prevailing negative surface charge of Δ*nifB*-Av1, which will be further accentuated by the approximately −7 net charge of the disordered loop, there is an evident accumulation of positive surface charge lining the funnel the entire way from the entrance down to the FeMoco binding site

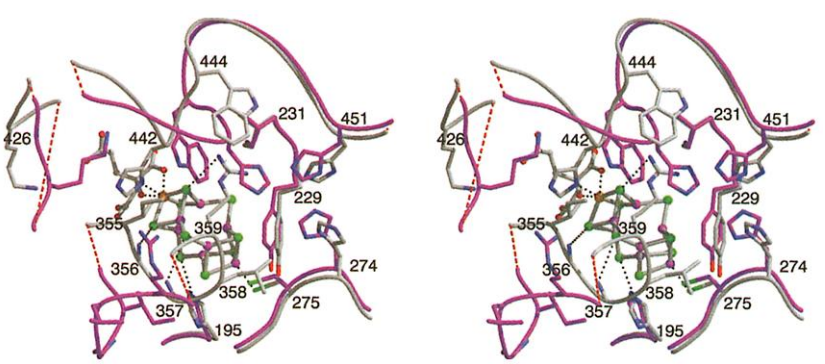

Fig. 3. Stereo view of the protein environment in the vicinity of the FeMoco, viewed from the MoFe protein surface. This figure shows part of the backbone and some side-chain residues (labeled only for Av1) in the α subunit, after superposition (*31*) of Δ*nifB*-Av1 and Av1 based on C_α positions in the β subunits. Atoms are color coded, with Mo in orange, Fe in purple, S in green, O in red, N in blue, and C in purple (Δ*nifB*-Av1) or gray (Av1). The FeMoco (including homocitrate) is represented as a ball-and-stick model. Black dotted lines indicate hydrogen-bond interactions with the FeMoco, and red dotted lines connect corresponding C_α atoms in domain αIII of Δ*nifB*-Av1 and Av1. The switching of positions of the side chains of His α442 and Trp α444 and the formation of a His triad in Δ*nifB*-Av1 are shown.

(Fig. 4A). This electrostatic feature presumably serves to steer the negatively charged FeMoco (*17*) into the correct position for the holoprotein. The loop from residues α353 to α364 (Figs. 2 and 3), which contains the positively charged residues Arg α359 and Arg α361, as well as His α362, is located at the entrance of the funnel. Additional Lys (α315 and α426), Arg (α96, α97, and α277), and His (α274, α442, and α451) residues in the funnel area create a positively charged environment and provide a path for the FeMoco insertion. The dominant contribution of the homocitrate to the negative charge of FeMoco suggests that the homocitrate/Mo end of the FeMoco will first enter the funnel, encountering His α442 at the bottom of the funnel as the initial Mo atom docking point. This initial binding of FeMoco could trigger a rearrangement in the positions of His α442/Trp α444 that leads to the formation of β strand 5, concomitant with the COOH-terminal extension of the other β strands, and subsequent closing up of the domain.

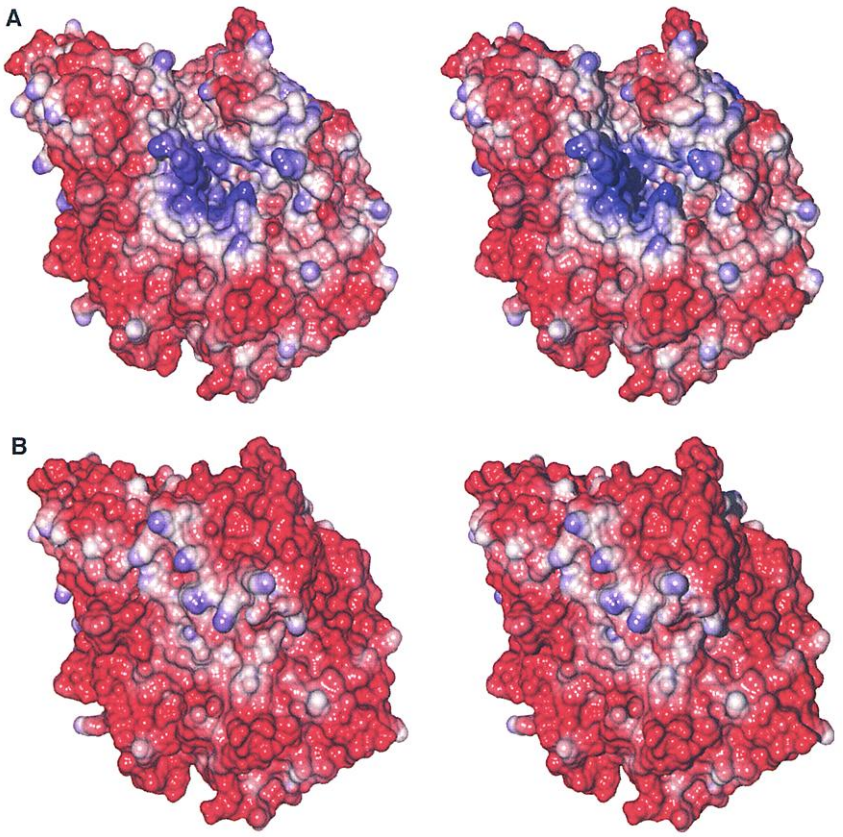

Fig. 4. (**A**) Electrostatic surface potential representation (stereo view) of a Δ*nifB*-Av1 αβ subunit pair viewed from an orientation similar to that in Fig. 1, B and C. Negative and positive potentials are shown in red (–10.0 *kT*) and blue (10.0 *kT*), respectively. (**B**) Surface representation of Av1, with the same parameters as in (A). The programs MSMS (*34*), SWISS PDB VIEWER (*35*), and POVRAY were used to prepare Fig. 4.

Table 1. Data collection and refinement statistics. Δ*nifB*-Av1 crystals grow in space group $C222_1$ (a = 150.5 Å, b = 191.9 Å, c = 102.3 Å) with one-half (αβ) of the $\alpha_2\beta_2$ tetramer in the asymmetric unit. Details of the crystallization and structure determination by molecular replacement are provided in the supplementary material (*28*).

*Data statistics**	
Resolution (Å)	30.0 to 2.3
Measured reflections	1,632,866
Unique reflections	60,354
Completeness (%)	91.6 (87.5)
$I/\sigma(I)$	15.7 (2.2)
R_{merge}† (%)	8.8 (44.0)
Refinement statistics	
R_{cryst}‡ (%)	24.9
R_{free}‡ (%)	28.9
Root mean square deviation of bond lengths (Å)	0.008
Root mean square deviation of bond angles (°)	1.38
Number of nonhydrogen atoms	
Protein§	7,399
Water molecules	241

*Values in parentheses are for the highest resolution shell: 2.38 to 2.30 Å. †$R_{merge} = \Sigma_{hkl}\Sigma_i|I_i - \langle I\rangle|/\Sigma_{hkl}\Sigma_i\langle I\rangle$, where I_i is the intensity of the ith measurement of a reflection with indices hkl and $\langle I\rangle$ is the weighted mean of all measurements of I. ‡$R_{cryst} = \Sigma_{hkl}||F_{obs}(hkl)| - k|F_{calc}(hkl)||/\Sigma_{hkl}|F_{obs}(hkl)|$ for the working set of reflections. R_{free} is R_{cryst} for 5% of the reflections excluded from the refinement. §Residues α1 to α48, α381 to α407, and α481 to α492 are disordered in Δ*nifB*-Av1; for comparison, residues α1 to α4, α36 to α44, and α481 to α492 are disordered in Av1.

Although the biosynthesis of nitrogenase is a particularly involved process because of the complexity of the metalloclusters, even for "simpler" metalloproteins, incorporation of transition metals into active sites involves the participation of multiple proteins to ensure proper uptake and distribution. This has been most clearly demonstrated for copper-containing proteins, where copper is delivered to the active site of target proteins through direct protein-protein interactions between the target and specialized proteins known as "metallochaperones" (*18–21*). The best characterized copper metallochaperones are found to be homologous to their target proteins. Formation of the target apoprotein-metallochaperone complex is mediated by subunit-subunit interactions that mimic those found in the holoprotein. As a result of this hetero-oligomeric association, the active site is opened for access by the metal coordinated to the metallochaperone, with subsequent transfer of metal between the two proteins, dissociation of the protein-protein complex, and reformation of the holoprotein oligomer. It has been suggested that this subunit exchange mechanism observed for copper-containing proteins may be a general feature of the interaction between target proteins and metallochaperones, including the assembly of proteins such as the MoFe protein (*21*).

The process of FeMoco incorporation into the cofactor-deficient MoFe protein exhibits intriguing similarities, as well as distinctive features, relative to these observations on copper-containing proteins. Both systems appear to share a common requirement for protein-protein interactions for incorporation of the metallocenter. Given the instability of the isolated FeMoco, it is likely that the biosynthetic pathway involves protein-bound species and not free cofactor; a number of proteins have been implicated as carrying precursors to FeMoco (*1, 4, 22*), including the NifEN protein that is homologous to the MoFe protein (*23*), although the penultimate carrier preceding incorporation into the MoFe protein has not been conclusively identified. It appears unlikely from the structure of Δ*nifB*-Av1 that cofactor insertion involves subunit-subunit exchange of the type documented for copper-containing proteins; the

αβ subunit interfaces are extensive, include the P cluster in both Δ*nifB*-Av1 and Av1, and should remain intact. However, the rearrangement of the αIII domain, in addition to generating the opening for FeMoco insertion, may also create a potential interaction domain that enables residues found in the disordered region of the Δ*nifB*-Av1 structure to dock with the FeMoco donor.

References and Notes

1. R. M. Allen, R. Chatterjee, M. S. Madden, P. W. Ludden, V. K. Shah, *Crit. Rev. Biotechnol.* **14**, 225 (1994).
2. B. K. Burgess, D. J. Lowe, *Chem. Rev.* **96**, 2983 (1996).
3. J. B. Howard, D. C. Rees, *Chem. Rev.* **96**, 2965 (1996).
4. B. E. Smith, *Adv. Inorg. Chem.* **47**, 159 (1999).
5. D. C. Rees, J. B. Howard, *Curr. Opin. Chem. Biol.* **4**, 559 (2000).
6. B. Schmid, H.-J. Chiu, V. Ramakrishnan, J. B. Howard, D. C. Rees, in *Handbook of Metalloproteins*, A. Messerschmidt, R. Huber, K. Wieghardt, T. L. Poulos, Eds. (Wiley, Chichester, UK, 2001), vol. 2, pp. 1025–1036.
7. J. Christiansen, D. R. Dean, L. C. Seefeldt, *Annu. Rev. Plant Physiol. Plant Mol. Biol.* **52**, 269 (2001).
8. J. Kim, D. C. Rees, *Nature* **360**, 553 (1992).
9. V. K. Shah, W. J. Brill, *Proc. Natl. Acad. Sci. U.S.A.* **74**, 3249 (1977).
10. The His-tag version of the *A. vinelandii* MoFe protein from a Δ*nifB* strain (DJ1143) contains eight His located between residues α3 and α4. Because an identically His-tagged version of an otherwise wild-type MoFe protein has full in vivo and in vitro activities, structural features that are critical for FeMoco insertion are not affected by this His-tag extension (*11*).
11. J. Christiansen, P. J. Goodwin, W. N. Lanzilotta, L. C. Seefeldt, D. R. Dean, *Biochemistry* **37**, 12611 (1998).
12. J. W. Peters *et al.*, *Biochemistry* **36**, 1181 (1997).
13. S. M. Mayer, D. M. Lawson, C. A. Gormal, S. M. Roe, B. E. Smith, *J. Mol. Biol.* **292**, 871 (1999).
14. A movie showing schematically the rearrangements in domain αIII between the structures of Δ*nifB*-Av1 and Av1 is available as supplemental material on Science Online at www.sciencemag.org/cgi/content/full/296/5566/352/DC1.
15. J. Kim, D. Woo, D. C. Rees, *Biochemistry* **32**, 7104 (1993).
16. Sequence conservation is based on a comparison of known nitrogenase MoFe protein sequences (SWISS-PROT) with the program BLAST (*24*).
17. Isolated FeMoco is known to be anionic (*25*). In the resting state of Av1, the core charge on the metals in FeMoco is proposed to be +1 (*26*) or +3 (*27*), with an overall negative charge supplied by homocitrate, which has a charge of −4 if the hydroxyl group is deprotonated.
18. V. C. Culotta *et al.*, *J. Biol. Chem.* **272**, 23469 (1997).
19. J. S. Valentine, E. B. Gralla, *Science* **278**, 817 (1997).
20. A. C. Rosenzweig, *Acc. Chem. Res.* **34**, 119 (2001).
21. A. L. Lamb, A. S. Torres, T. V. O'Halloran, A. C. Rosenzweig, *Nature Struct. Biol.* **8**, 751 (2001).
22. P. Rangaraj, C. Rüttimann-Johnson, V. K. Shah, P. W. Ludden, *J. Biol. Chem.* **276**, 15968 (2001).
23. K. E. Brigle, M. C. Weiss, W. E. Newton, D. R. Dean, *J. Bacteriol.* **169**, 1547 (1987).
24. S. F. Altschul, W. Gish, W. Miller, E. W. Myers, D. J. Lipman, *J. Mol. Biol.* **215**, 403 (1990).
25. B. K. Burgess, *Chem. Rev.* **90**, 1377 (1990).
26. H.-I. Lee, B. J. Hales, B. M. Hoffman, *J. Am. Chem. Soc.* **119**, 11395 (1997).
27. S. J. Yoo, H. C. Angove, V. Papaefthymiou, B. K. Burgess, E. Münck, *J. Am. Chem. Soc.* **122**, 4926 (2000).
28. Supplementary information on the methods used is available on *Science* Online [see (*14*) for URL].
29. P. J. Kraulis, *J. Appl. Crystallogr.* **24**, 946 (1991).
30. E. A. Merritt, D. J. Bacon, *Methods Enzymol.* **277**, 505 (1997).
31. G. J. Kleywegt, *Acta Crystallogr.* **D52**, 842 (1996).
32. Single-letter abbreviations for the amino acid residues are as follows: A, Ala; C, Cys; D, Asp; E, Glu; F, Phe; G, Gly; H, His; I, Ile; K, Lys; L, Leu; M, Met; N, Asn; P, Pro; Q, Gln; R, Arg; S, Ser; T, Thr; V, Val; W, Trp; and Y, Tyr.
33. W. Kabsch, C. Sander, *Biopolymers* **22**, 2577 (1983).
34. M. F. Sanner, A. J. Olson, J.-C. Spehner, *Biopolymers* **38**, 305 (1996).
35. N. Guex, M. C. Peitsch, *Electrophoresis* **18**, 2714 (1997).

36. This work was supported by NIH (B.K.B, D.R.D., and D.C.R.) and by a Deutsche Forschungsgemeinschaft research fellowship (B.S.). The rotation camera facility at the Stanford Synchrotron Radiation Laboratory is supported by the U.S. Department of Energy and NIH. Coordinates have been deposited with the Protein Data Bank (accession code 1L5H). Dedicated to the memory of Barbara K. Burgess (1 January 1951 to 30 December 2001).

18 January 2002; accepted 12 March 2002

Outbreak of Poliomyelitis in Hispaniola Associated with Circulating Type 1 Vaccine-Derived Poliovirus

Olen Kew,[1]* Victoria Morris-Glasgow,[2] Mauricio Landaverde,[3] Cara Burns,[1] Jing Shaw,[1] Zacarías Garib,[4] Jean André,[5] Elizabeth Blackman,[2] C. Jason Freeman,[1] Jaume Jorba,[1] Roland Sutter,[6] Gina Tambini,[3] Linda Venczel,[3] Cristina Pedreira,[7] Fernando Laender,[8] Hiroyuki Shimizu,[9] Tetsuo Yoneyama,[9] Tatsuo Miyamura,[9] Harrie van der Avoort,[10] M. Steven Oberste,[1] David Kilpatrick,[1] Stephen Cochi,[6] Mark Pallansch,[1] Ciro de Quadros[3]

An outbreak of paralytic poliomyelitis occurred in the Dominican Republic (13 confirmed cases) and Haiti (8 confirmed cases, including 2 fatal cases) during 2000–2001. All but one of the patients were either unvaccinated or incompletely vaccinated children, and cases occurred in communities with very low (7 to 40%) rates of coverage with oral poliovirus vaccine (OPV). The outbreak was associated with the circulation of a derivative of the type 1 OPV strain, probably originating from a single OPV dose given in 1998–1999. The vaccine-derived poliovirus associated with the outbreak had biological properties indistinguishable from those of wild poliovirus.

The last case of poliomyelitis in the Americas associated with circulating indigenous wild poliovirus was reported in Peru in 1991 (*1*). The last poliomyelitis cases in the Caribbean occurred on the island of Hispaniola, which is divided between the Dominican Republic (where the last reported case was in 1985) and Haiti (where the last reported case was in 1989). Since 1992, investigation of nearly 20,000 cases of acute flaccid paralysis (AFP) throughout the Americas (*2*) has found only sporadic cases of vaccine-associated paralytic poliomyelitis (VAPP) (*3*). The only known wild poliovirus infections in the Americas after 1991 were associated with importations into Canada (*4*, *5*). Neither of these importations was associated with paralytic disease, and there was no evidence of the spread of the virus to the wider community.

In the summer of 2000, cases of AFP were reported from Bonao, Dominican Republic (date of onset: 12 July), and Port-de-Paix, Haiti (date of onset: 28 August), communities that are separated by ~300 km (Fig. 1) (*6*). Stool specimens collected from the patients were positive for poliovirus type 1. An initial characterization of the isolates by nucleic acid probe hybridization (*7*) indicated that they were vaccine-derived poliovirus (VDPV). In countries using oral poliovirus vaccine (OPV), VDPV is occasionally isolated from the stools of patients with nonpolio AFP (*2*, *3*). However, several observations raised concerns that the AFP cases in Hispaniola might be caused by

[1]Division of Viral and Rickettsial Diseases, National Center for Infectious Diseases, Centers for Disease Control and Prevention (CDC), 1600 Clifton Road, Atlanta, GA 30333, USA. [2]Caribbean Epidemiology Centre (CAREC) Laboratory, Pan American Health Organization (PAHO), 16-18 Jamaica Boulevard, Federation Park, Port-of-Spain, Trinidad and Tobago. [3]Division of Vaccines and Immunization, PAHO, 525 Twenty-Third Street, N.W., Washington, DC 20037, USA. [4]Ministry of Health, Avenida San Cristóbal esquina Tiradentes, Santo Domingo, Dominican Republic. [5]Ministry of Public Health, Port-au-Prince, Haiti. [6]Vaccine Preventable Disease Eradication Division, National Immunization Program, CDC, 1600 Clifton Road, Atlanta, GA 30333, USA. [7]PAHO, Calle Pepillo Salcedo, Plaza de la Salud, Santo Domingo, Dominican Republic. [8]PAHO, Number 295 Avenue John Brown, Port-au-Prince, Haiti. [9]Department of Virology II, National Institute of Infectious Diseases, Toyama 1-23-1, Shinjuku-ku, Tokyo 162, Japan. [10]Polio Laboratory, National Institute of Public Health and the Environment (RIVM), Antonie van Leeuwenhoeklaan 9, 3720 BA, Bilthoven, Netherlands.

*To whom correspondence should be addressed. E-mail: okew@cdc.gov